PCCP

Accepted Manuscript

ROYAL SOCIETY OF CHEMISTRY

www.rsc.org/pccp

Structural, electronic, magnetic and chemical properties of B-, C- and N-doped MgO(001) surface

Igor A. Pašti[1], Natalia V. Skorodumova[2,3]

[1]*University of Belgrade, Faculty of Physical Chemistry, Studentski trg 12-16, 11158 Belgrade, Serbia*

[2]*Department of Materials Science and Engineering, School of Industrial Engineering and Management, KTH - Royal Institute of Technology, Brinellvägen 23, 100 44 Stockholm, Sweden*

[3]*Department of Physics and Astronomy, Uppsala University, Box 516, 751 20 Uppsala, Sweden*

***corresponding author:**

Dr. Igor A. Pašti, assistant professor

University of Belgrade, Faculty of Physical Chemistry

Studentski trg 12-16, 11158 Belgrade, Serbia

Phone: +381 11 3336 628

Fax: +381 11 2187 133

E-mail: igor@ffh.bg.ac.rs

Abstract

Doping of simple oxide materials can give rise to new exciting physical and chemical properties and open new perspectives for a variety of possible applications. Here we use Density Functional Theory calculations to investigate the B-, C- and N-doped MgO(001) surfaces. We have found that the investigated dopants induce magnetization of the system amounting to 3, 2 and 1 μ_B for B, C and N, respectively. The dopants are found to be in the X^{2-} state and tend to segregate to the surface. These impurity sites also present the centers of altered chemical reactivity. We probe the chemisorption properties of the doped MgO(001) surfaces with the CO molecule and atomic O. The adsorption of CO is much stronger on B- and C-doped MgO(001) compared to pure MgO(001) as the impurity sites serve as potent electron donors. The situation is similar for the case of atomic oxygen, for which we find the adsorption energy of −8.78 eV on B-doped MgO(001). The surface reactivity changes locally around the dopant atom, being mainly restricted to its first coordination shell. The presented results suggest doped MgO as a versatile multifunctional material with possible use as adsorbent or catalyst.

Keywords: magnesium oxide, surface doping, magnetism, reactivity, CO adsorption

1. Introduction

Constant search for materials with desired properties is one of the tasks of contemporary materials science and the basis for advancement of modern technologies. Tailoring materials properties to applications is one of the strategies for this search, which led to successful development of novel materials over the years. In particular, tuning surfaces by introducing defects,[1] surface overlayers[2,3] or doping[4,5] gave rise to outstanding new properties compared to those of unmodified materials.

In general, the variability of the surface properties of metal oxides makes them useful for different research fields and technological areas, such as, energy conversion,[6] chemical sensors and environmental monitoring,[7] ceramics,[8] corrosion,[9] catalysis[10,11] and others. For example, due to its simple rock salt structure, strong ionic bonding, small surface relaxation, simplicity in preparation and good chemical stability magnesium oxide is widely used in surface science. Moreover, magnesia surface displays rather poor reactivity even in reactions with atomic species[12] that makes it a good catalyst support for numerous catalytic reactions.[10,11,13–15] On the other hand, the properties of MgO surface can be modified, when required, by introducing defects or impurities[16–19], or underlying metal substrate.[20–23]

Recently, d^0 magnetism has been demonstrated for N-doped MgO.[24,25] Grob *et al*. produced N-doped MgO films on Mo substrate and confirmed such a behavior.[26] Additionally, theoretical calculations based on density functional theory (DFT) suggest that N tends to exchange places with O in the MgO lattice.[26] Pesci *et al*. provided a detailed theoretical description of N-doped bulk MgO using DFT and suggested that the formation of substitutional and interstitial N sites in MgO depended on oxygen concentration and other conditions during the preparation.[27] The theoretical work by Shein *et al*. also predicted the appearance of magnetization in the case of C-

doped multi-walled MgO nanotubes assuming C→O substitution.[28] In fact, the authors suggested that magnetism will appear if the valence orbitals of a dopant lie above the occupied O 2p band of the matrix, and proposed B, C and N as possible dopants for the production of the MgO-based magnetic materials.[28] Also, Kenmochi *et al*. has indeed considered B-, C- and N-doped CaO as a new class of diluted magnetic semiconductors.[29]

In this paper we report our results on the MgO(001) surface doped with B, C and N. We analyze the electronic properties of such surfaces, tendency to surface segregations and appearance of magnetism in these systems. Moreover, knowing that doping of MgO can significantly alter its reactivity[30] we probe the chemisorption properties of the doped MgO(001) surfaces towards molecular and atomic adsorption using the CO molecule and atomic O.

2. Computational details

The calculations were based on DFT within the generalized gradient approximation (Perdew–Burke–Ernzerhof exchange correlation functional[31]). The calculations were performed using the Quantum ESPRESSO *ab initio* package[32] using ultrasoft pseudopotentials where only the s- and p- states of all atoms were treated as the valence states. The kinetic energy cutoff for the plane-wave basis set was 28 Ry and the charge density cutoff was 16 times higher, for all the calculations. Spin polarization was taken into account for all the investigated systems. The calculated equilibrium lattice constant was 4.22 Å, in good agreement with the experimental value of 4.21 Å.[33] The MgO (001) surface was modeled by a 2x2 four layer thick slab, which had eight magnesium and eight oxygen atoms per atomic layer. One dopant atom *per* simulation cell was introduced, thus giving the total dopant concentration of 1.56 at. %. The concentration in the layer was 12.5% and the distance between the dopant and its image was 8.44 Å. All the atoms in

the MgO(001) slab were relaxed, except for the first bottom layer which was fixed during the geometry optimization. The first irreducible Brillouin zone was integrated using a 4×4×1 Monkhorst-Pack grid.[34] A Gaussian smearing procedure, with the broadening of 0.007 Ry, was applied. The surface slabs were separated by a vacuum region of 18 Å. The dipole correction was added to prevent any interactions along the z direction.[35] The charge transfer was analyzed using the Bader algorithm[36] on a charge density grid by Henkelman *et al.*[37]

In order to address the energetics of the replacement of oxygen in MgO lattice with a dopant X (X = B, C or N; we shall use "X" hereafter to denote the dopant atoms) we define the substitution energy (E_{sub}(X)) as:

$$E_{sub}(X) = (E_{X-MgO} + E_O) - (E_{MgO} + E_X) \quad (1)$$

In the equation above $E_{X\text{-}MgO}$ and E_{MgO} stand for the total energies of X-doped MgO(001) and pristine MgO(001). E_O and E_X denote the total energies of the isolated O and X atoms, respectively. Alternatively, the incorporation of X into MgO lattice can be considered as the binding of atom X on the oxygen vacancy, which can be quantified as the binding energy (E_b(X)):

$$E_b(X) = E_{X\text{-}MgO} - (E_{v\text{-}MgO} + E_X) \quad (2)$$

where $E_{v\text{-}MgO}$ denotes the total energy of the MgO(001) surface with an oxygen vacancy.

In this work we also address the chemisorption properties of the X-doped MgO(001) surface towards CO and atomic O. The chemisorption of a given adsorbate A is quantified here as the adsorption energy (E_{ads}(A)), defined as:

$$E_{ads}(A) = E_{X\text{-}MgO+A} - (E_{X\text{-}MgO} + E_A) \quad (3)$$

where $E_{X\text{-}MgO+A}$, and E_A stand for the total energy of the systems with the adsorbate, and the total energy of the isolated adsorbate, respectively. Please note that in Eq. (3) we do not include the dissociation energy of molecular O_2 into E_{ads}, instead it is calculated with respect to the energy of an isolated O atom. We probe the adsorption at different sites of the doped MgO(001) surface and the notations of the adsorption sites, used hereafter, are presented in Fig. 1.

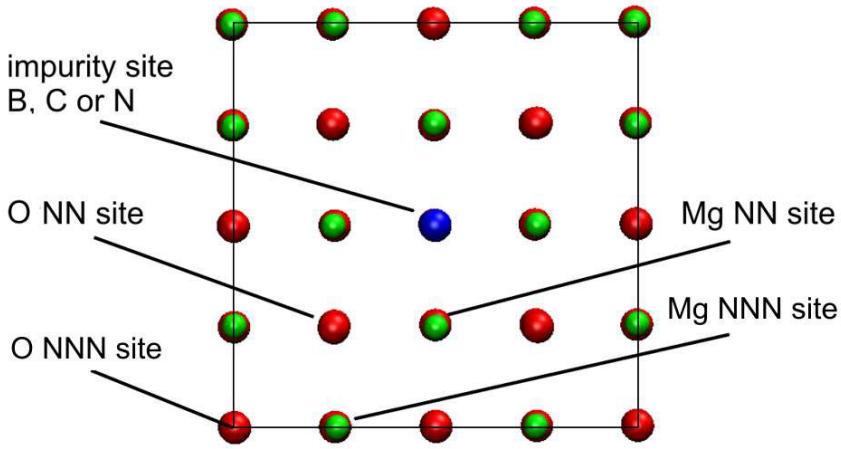

Figure 1. Notation of the adsorption sites at doped MgO(001) surface within the simulation supercell (NN – Nearest Neighbour, NNN – Next Nearest Neighbor). Graphical presentation was made using the VMD code.[38]

3. Results

3.1. Structural, electronic and magnetic properties of X-doped (X = B, C, N) MgO(001)

A surface structure of an oxide can be characterized by the relaxation and rumpling parameters. The surface relaxation parameter (δd_{12}, in %) can be defined as:

$$\delta d_{12} = \frac{d_{12} - d}{d} \times 100 \qquad (4)$$

where d_{12} stands for the averaged vertical distance between the first and the second surface layer and d is the interlayer distances in the bulk. Surface rumpling (Δ_1) can be defined as:

$$\Delta_1 = \frac{z_O - z_{Mg}}{d} \times 100 \quad (5)$$

where $z_{O(Mg)}$ stands for the vertical position of the O(Mg) atoms in the surface layer. Earlier calculations performed for MgO(001) produced δd_{12} = +0.10 % and Δ_1 = +2.50 %. Thus, the surface relaxation is very small and the oxygen atoms of the first surface layer are situated slightly above the Mg surface atoms. The calculated values are in harmony with the experimentally measured ones using vacuum cleaved MgO(001).[39–41] As a comparison, previous DFT calculations estimated the values of δd_{12} and Δ_1 to +0.003% and 2.27%, respectively.[42]

Next we turn to doped MgO(001). We look at the case of substitutional doping when B, C or N replace an O atom in the surface layer or subsurface layer of the MgO(001) slab. By comparing the total energies of doped MgO(001) for the two different dopant positions (Fig. 2, insets A and B), we observe that all the three dopants prefer to be in the surface layer (Fig. 2, inset A). This indicates a tendency for dopants to segregate on the surface, while the energy cost for placing X into the subsurface layer of MgO(001) decays as X approaches oxygen in the Periodic Table of Elements (PTE).

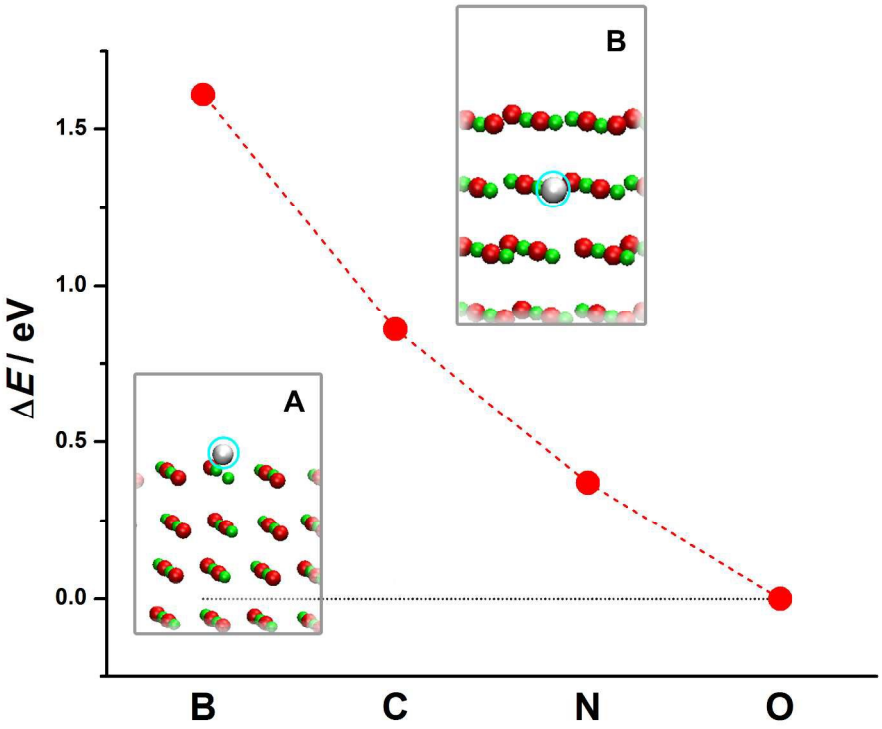

Figure 2. Energy cost for the exchange of X between the surface (structure A) and subsurface layer of MgO(001) (structure B).

The formation of X-doped MgO(001) can be considered either as the replacement of oxygen with atom X or as the adsorption of atom X at a vacancy site. In the first case, a large energy input is required to replace O with X and it decays as X approaches O in the PTE (Table 1). Hence, healing of the surface vacancy site with oxygen will be preferred over the healing with B, C or N. However, if looking at the formation of X-MgO(001) as the adsorption of X at the O vacancy, than this process is followed by deliberation of a large amounts of energy (Table 1). As the adsorption of X at an O vacancy site is more exothermic than adsorption on the MgO(001) terrace,[12] the investigated dopants are expected to be entrapped by vacancies when no oxygen is available to heal the surface. This agrees with the results of Pesci *et al*. who suggested that the substitutional doping of MgO with N can be realized under oxygen-poor conditions.[26]

Table 1. Energetic (substitution energy and binding energy of X at the surface vacancy site), structural (X atom vertical shift and interatomic distances in the surface layer) and magnetic parameters of the B-, C- and N-doped MgO(001). Binding energies are calculated as the binding of the atom X at the surface O vacancy site of MgO(001). Total magnetization (M) and magnetization of the impurities (M_X) are given. At the end, charge transferred to the dopant (Q_X) atom is given.

dopant X	E_{sub}(X) / eV[a]	E_b(X) / eV[b]	Δ_X / %	d(X-Mg) / Å	d(X-O) / Å	M / μ_B	M_X / μ_B	Q_X / e
B	5.91	−3.46	42.2	2.37	3.17	3	2.20	1.97
C	4.29	−5.08	19.3	2.23	3.02	2	1.62	1.98
N	3.89	−5.48	10.8	2.16	3.04	1	0.88	1.99
O[c]	0	−9.37	0.05	2.11	2.99	0	0	1.99

[a]subsitution energy according to Eq. (1); [b]binding of X at the O vacancy site according to Eq. (2); [c]corresponds to pristine MgO(001)

Here we can conclude that the adsorption of the investigated elements at the O vacancy site becomes more exothermic as the position of the doping element in the PTE approaches that of oxygen. The adsorption of an O atom at an O vacancy site, restores perfect MgO(001) and E_b(O), in this case, equals −9.37 eV. This process is actually reversed to the vacancy formation and its energy balance is in good agreement with the results of Carrasco *et al*. who found the surface vacancy formation energy to be in the range of 9.31 – 9.42 eV, depending on the number of MgO layers in the surface model.[43] For comparison, we estimate the formation energy of the subsurface vacancy to be 9.87 eV, which is identical to the result of the Carrasco *et al*. for the 3-layers MgO(001) slab.[43] The same authors estimated this quantity to 9.97 eV using 12 layer model. The preference for the lower coordinated surface sites, observed for the investigated

dopants, is in line with the results reported for C-doped MgO nanotubes.[28] This preference is not due to the difference between the formation energies of surface and subsurface oxygen vacancies. When we calculated the interaction energy between dopant X and the subsurface vacancy, we saw that it was always smaller compared to the interaction with the surface vacancy site.

To characterize the impurity site, we define vertical shift of the atom X as:

$$\Delta_X = \frac{z_X - z_1}{d} \times 100 \qquad (6)$$

where $z_X - z_1$ gives the difference between the vertical positions of atom X and the average vertical position of other atoms in the surface layer. These data are provided in Table 1, along with the distances between X and the nearest Mg and O atoms (d(X-Mg) and d(X-O)). We see that the shift of the dopant decreases from B to C and further to N.

The dopant atoms induce the magnetization of the system mostly at the impurity site. The total magnetization (Table 1) decays from 3 μ_B (B-doping) to 2 μ_B (C-doping) and to 1 μ_B (N-doping). For C and N the magnetizations match the ones observed in the cases of the adsorption of these atoms on perfect MgO(001).[12] For boron the situation is different as the magnetic moment is 3 μ_B in the case of substitution and 1 μ_B in the case of adsorption. However, if the magnetization of the B-doped MgO(001) is forced to 1 μ_B the energy of the system increases by 0.44 eV. The difference is even greater (1.59 eV) for subsurface B-doping. Moreover, the magnetic solutions for X-doped MgO(001) are significantly more stable than non-magnetic ones, with the energy difference amounting to 0.66, 0.88 and 0.39 eV for B-, C-, and N-doped MgO, respectively.

The analysis of Bader charges shows that in all the considered cases nearly 2 electrons are transferred to the dopant atoms (Table 1) indicating that the dopants are in the X^{2-} state. Even

though B, C and N have lower electronegativity compared to O it is still sufficient to attract the valence electrons of Mg atoms. When a dopant atom receives electrons from neighboring Mg atoms its electron shell expands. As B has smaller core charge than C and N, for the same amount of donated charge its electron shell will expand more. Considering atoms/ions in MgO as touching spheres the ionic radii of B, C and N in doped MgO(001) can be estimated as 1.675, 1.615 and 1.545 Å, respectively, all of them being larger than that of O^{2-} in MgO (1.499 Å). These considerations offer a simple explanation of the tendency of the dopant atoms to prefer the surface layer of MgO(001). As X^{2-} ions are larger compared to O^{2-}, their introduction into the MgO lattice induces larger strain when placed into subsurface layers, therefore, their migration to the surface layer brings some strain relief. To check this assumption we calculated the deformation energy of the MgO lattice when a dopant is placed into the surface or subsurface layer (Fig. 3). The deformation energy (ΔE) is calculated here as the difference between the energy of the relaxed X-doped MgO(001) surface when dopant atom is removed and the corresponding energy when O atom is removed from pristine MgO(001) (from the surface or subsurface layer). The deformation energy is smaller for the surface doped structures than that for the subsurface ones and it decreases as the ionic radius of the dopant approaches the ionic radius of O^{2-} ion.

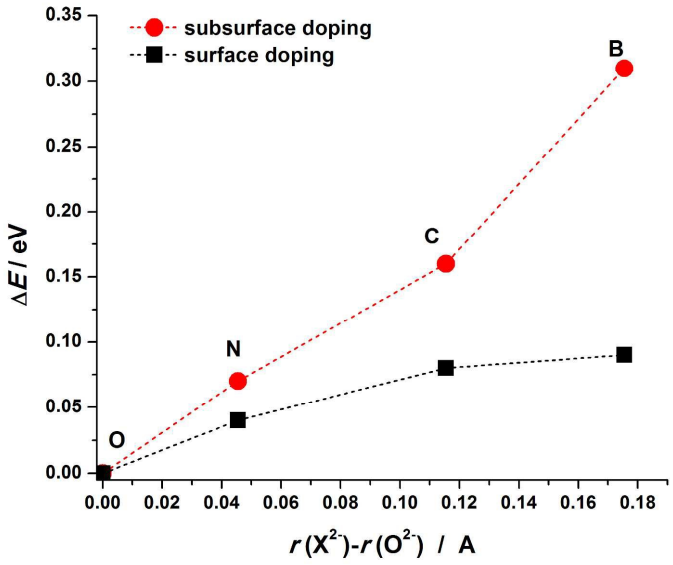

Figure 3. Deformation energy of the MgO lattice (ΔE) upon the incorporation of the investigated dopants into the surface vacancy (squares) and the subsurface vacancy (circles).

The observed charge transfer also provides an intuitive explanation for the observed magnetizations. Formally, when boron (which has one unpaired electron) receives 2 electrons, the total number of unpaired electrons becomes 3 that matches the observed magnetization of the system. In the case of nitrogen, the electron transfer induces electron pairing and only one unpaired electron is left (M = 1 μ_B). This is, of course, a rather simplified view, but it is clear that the magnetic moment is not associated with the charge transfer but the occupancy of the dopant band. The magnetizations calculated by us agree well with those provided by Shein *et al*. for the C-doped triple-walled square-prismatic MgO nanotube[28] as well as with the calculations of Grob *et al*.[26] for N-doped MgO. Considering our results and the ones published so far one can conclude that the rise of magnetization is rather localized to the impurity site. For C-doped MgO nanotubes the atomic magnetic moments of the C atoms at the surface are 1.815 - 1.682 μ_B,[28] while we found 1.62 μ_B for carbon dopant using Löwdin population analysis.[44,45] The

magnetization of the system is then complemented to an integer number by the contributions of dopant neighbors. Such a behavior is clearly evident from the spin density maps (Fig. 4, right), which show that the magnetization is localized at the dopant atom. In the case of subsurface doping we also observe that the atomic magnetic moments of the dopants in these systems are slightly smaller than those found for the surface doping, which is also in agreement with available reports.[28]

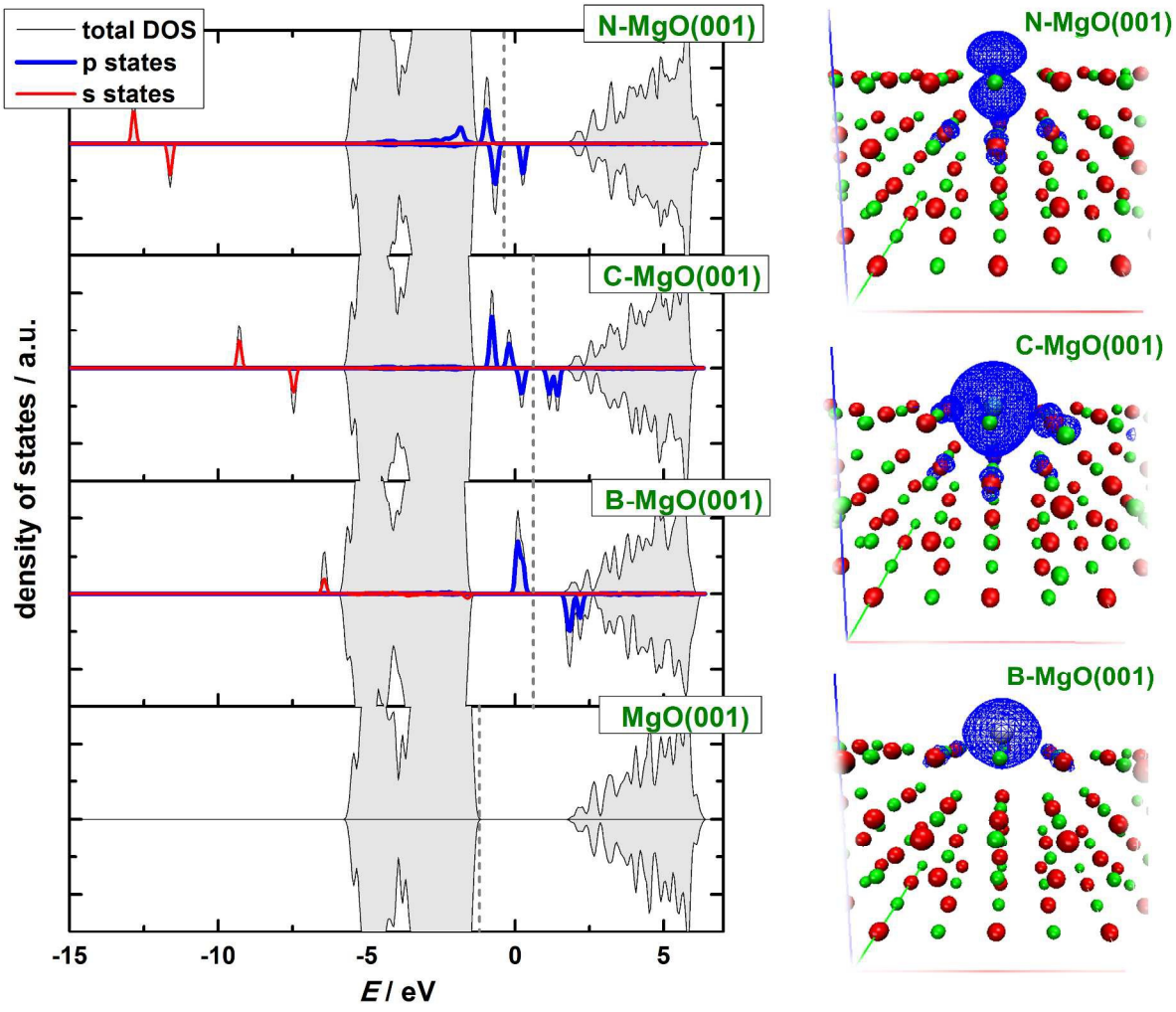

Figure 4. Left: Electronic structure of the X-doped MgO(001) surface (total DOS, shaded, and the s and p states of the dopant atoms) and the electronic structure of perfect MgO(001) (bottom). The highest occupied state is indicated by the vertical dashed line. Right: 3D spin

density (spin polarization) maps ($\rho_{\text{spin up}} - \rho_{\text{spin down}}$) are given for X-MgO(001) surfaces.

Inspecting the electronic structures of X-doped MgO(001) (Fig. 4), one can see that the magnetizations of the systems are due to the partially filled p states of dopants situated in the band gap of MgO(001). The spin up p states of the dopant atoms are filled, while the spin down states are partially unoccupied, giving rise to the magnetization of the system (Fig. 4). This agrees with the observation of Ref.[28]. The calculated electronic structure of N-doped MgO(001) qualitatively agrees with the results of Grob *et al*. for N-doped MgO.[26] The quantitative differences between our results are due to the different levels of theory which have been applied. Namely, in Ref.[26] the DFT+*U* approach has been used. The calculated electronic structure of N-MgO(001) also qualitatively agrees with the one given in Ref.[27] for the case of substitutional N^{2-} in bulk MgO for the identical concentration of N as considered here. Our results suggest that the investigated substitutionally doped MgO(001) surfaces retain the insulating nature of parental MgO(001), in spite of the fact that the applied GGA-PBE approach underestimates the band gap significantly (calculated value of the band gap is 2.9 eV) compared to experimental values. Namely, electron-energy-loss spectroscopy determined the gap of 6.15-6.2 eV[46], while the value of 7.8 eV was found from the electronic sprectrum of single-crystal MgO.[47]

In order to visualize the 2p band of the dopants we have plotted the Integrated Local Densities of States (ILDOS, Fig. 5). These bands are indeed located mostly at the dopant sites, with a very small contribution of the nearest O atoms. In the case of B and C doping, the 2p states have nearly spherical symmetry around the dopant atom. In the case of N, however, ILDOS has a donut shape oriented in the (001) surface plane. The spherical symmetry of the 2p states for the case of C doping was also observed in Ref.[28].

At the end of this section it is important to address potential ferromagnetic ordering in this class of materials. Pesci *et al.*[27] suggested that a high degree of spin localization may hinder the formation of ferromagnetic order at room temperature. On the other hand, Gross *et al.*[26] demonstrated that N-doped MgO(001) film on Mo acts as a ferromagnetic d^0 insulator.

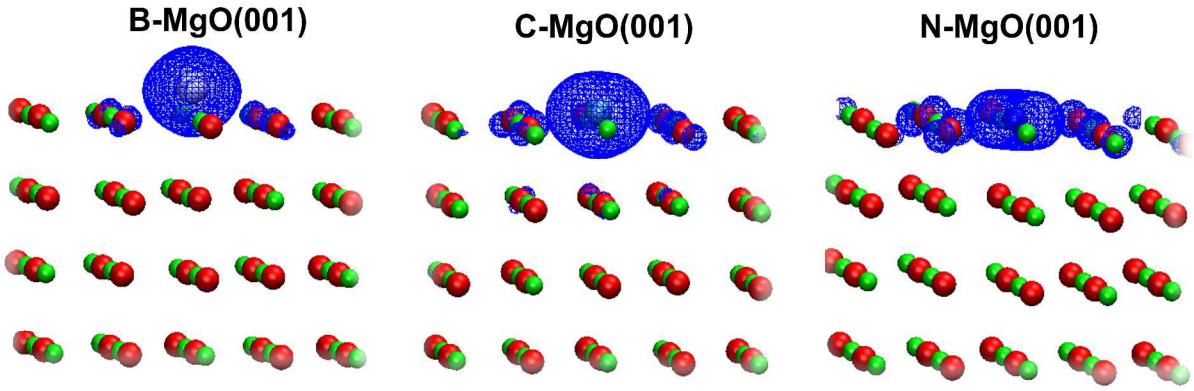

Figure 5. 3D ILDOS maps of filled X 2p like bands for the cases of B-doped (left), C-doped (middle) and N-doped MgO(001) (right). The total ILDOS between the MgO valence band and the highest occupied state are given and the width of the energy window chosen for the integration depends on the type of the X-doped MgO(001) (see Fig. 4).

3.2. Molecular adsorption on X-doped (X=B,C,N) MgO(001): CO case

As B, C and N incorporated into the MgO(001) surface have a number of unpaired electrons they can be in a sense regarded as radical species. Hence, these impurity sites can be centers of altered reactivity which might open a possibility to use such doped surfaces as adsorbents, catalysts, and so on. Pure MgO(001) surface is non-magnetic and rather inert. The question we want to answer here is whether the reactivity of the surface can be tuned by the introduction of the investigated impurities.

First we consider the CO/MgO(001) system, which attracted a lot of attention as being problematic for conventional DFT, requiring a special treatment and being looked at as a benchmark for the development of advanced theoretical methods.[48] Bonding of CO to MgO(001) is rather weak and the dispersion interaction contributes significantly to the adsorption energy.[49] Experimentally, it has been found that CO interacts with the Mg sites of the MgO(001) surface with the adsorption energy of −0.13 eV,[50] which qualifies the C-MgO(001) interaction as physisorption. Here we found the adsorption energy of −0.16 eV (Table 2), in good agreement with the experimental value, theoretical studies applying similar level of theory[10] as well as the computational study of Civalleri *et al*.[51] who applied modified B3LYP hydrid functionals to account for the dispersion interaction. When CO is bonded to the Mg site the C–O bond remains practically the same as in an isolated CO molecule, while the distance between the Mg center and the C atom is 2.43 Å (Table 2). The latter value is slightly smaller compared to those published previously, 2.489 - 2.578 Å, varying depending on the level of theory.[51] Using the Bader analysis we observed a small charge transfer to the CO molecule (0.09 e). For comparison, in Ref.[10] 0.10 e was found to be transferred to the CO molecule.

Now, let us turn to the CO chemisorption on X-doped MgO(001). The interaction of the CO molecule with B- and C-doped MgO(001) is mediated by the impurity site, the preferred one for bonding CO (Table 2). The strength of this interaction is remarkable: in the case of C-doped MgO(001) the CO adsorption energy is −5.08 eV. In both cases the total magnetization of the system is reduced by 2 μ_B. Another striking phenomenon is a tremendous charge transfer to the CO molecule. It results in a significant elongation of the C–O bond (Table 2), suggesting that B and C dopants act as potent electron donors. In contrast to the B and C cases, when MgO(001) is doped with N there is no interaction between the CO molecule and the impurity site. This seems

rather unexpected, but can be explained by ILDOS of the N-doped surface (Fig. 4, right), which demonstrates that the N 2p-orbirals are oriented in the surface plane, so the overlap between these states and the CO orbitals cannot be large. In the case of N-doped MgO(001) we have found that the stable adsorption site is the first Mg neighbor of the dopant (Mg NN site, Fig. 1) with the adsorption energy practically the same as for ideal MgO(001) (Table 2). In contrast, these sites are not stable on B- and C-doped MgO(001) and CO molecule goes to the impurity site during the structural relaxation. When moving away from the impurity site, a stable adsorption of the CO molecule is possible at the Mg sites, with the adsorption energies and charge transfer similar to those on defect-free MgO(001). Hence, we conclude that the effects of the dopant atoms on the CO adsorption are practically localized to the first coordination shell of the dopant.

Table 2. Energetic and structural parameters of the CO adsorption on pure and X-doped MgO(001) surface. Total magnetization (M) and the amount of the charge transferred to the adsorbate (ΔQ_{CO}) are included. Mg NN site is the nearest Mg neighbor of X site, and Mg NNN site is the next nearest Mg neighbor of the X impurity site.

Ads. Site	**System**	E_{ads}**(CO) / eV**	***d*(C–O) / Å**	***d*(C–Su)[a] / Å**	***M*** **/ μ_B**	ΔQ_{CO} **/ e**
Mg site	CO@MgO(001)	−0.16	1.14	2.43	0	0.09
Impurity site	CO@B-MgO(001)	−3.40	1.19	1.43	1	1.83
	CO@C-MgO(001)	−5.08	1.20	1.31	0	2.27
	CO@N-MgO(001)	0[b]	1.14	> 3.5	1	0.00
Mg NN site	CO@B-MgO(001)	ns[c]	-	-	-	-
	CO@C-MgO(001)	ns[c]	-	-	-	-

	CO@N-MgO(001)	−0.17	1.15	2.43	1	0.10
	CO@B-MgO(001)	−0.19	1.14	2.47	3	0.08
Mg NNN site	CO@C-MgO(001)	−0.16	1.14	2.44	2	0.09
	CO@N-MgO(001)	−0.15	1.14	2.45	1	0.09

[a]Su denotes surface atom at the CO adsorption site; [b]repulsive interaction; [c]not stable, relaxes to the impurity site

The electronic structure of the N-doped surface upon the CO adsorption (Fig. 6) demonstrates the absence of surface molecule interaction, while in the case of pure MgO(001) there is a very small overlap of the CO 2π states with the valence band of MgO(001). However, when MgO(001) is doped with B or C, there is a pronounced interaction between the impurity states and the CO molecule states, while the s and the p states of the dopants get hybridized (Fig. 6).

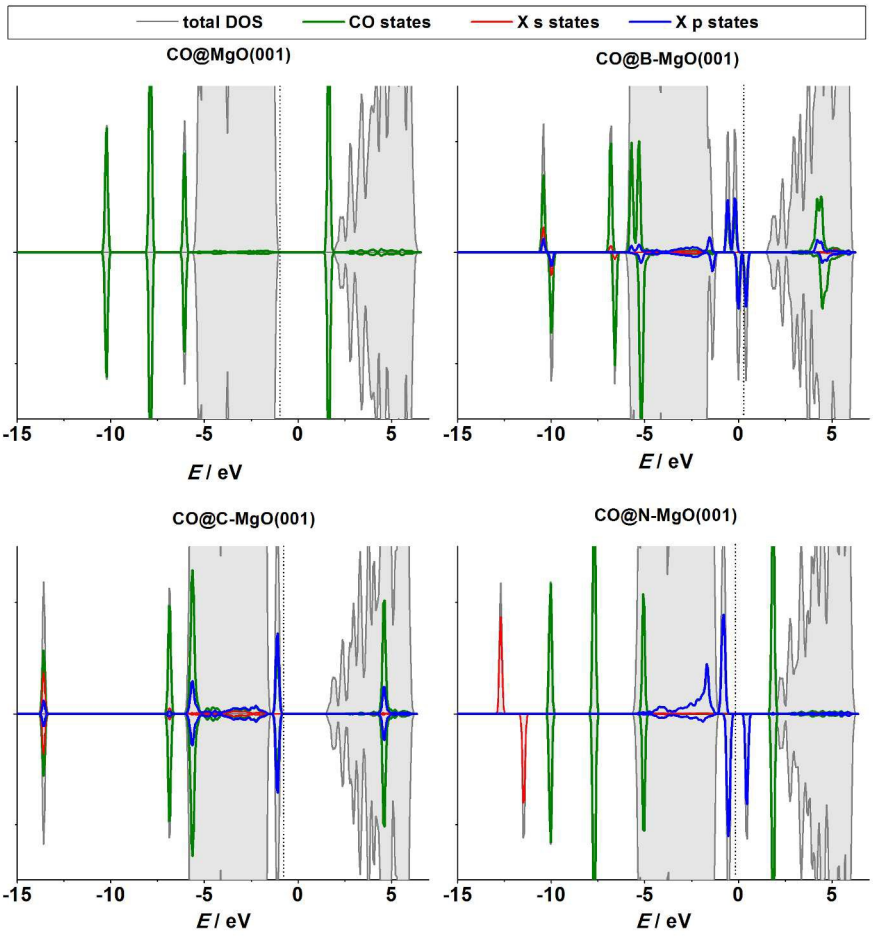

Figure 6. Projected densities of states for the case of the CO adsorption at the Mg site of the ideal MgO(001) and the impurity sites of the X-doped MgO(001) surface. Total densities of states are also included. Vertical lines indicate the highest occupied states.

299

300 3.3. Atomic adsorption on X-doped (X = B, C, N) MgO(001): O case

301 In its ground state, the atomic oxygen is a radical with two unpaired 2p-electrons. As a result, it
302 is very reactive but its adsorption on defect-free MgO(001) is relatively weak with E_{ads}(O)
303 calculated to be −2.16 eV (GGA-PBE).[12] Using B3LYP a somewhat smaller value, −1.91 eV,
304 was obtained by Di Valentin *et al.*[52] Considering the extreme reactivity of atomic O this is a
305 rather small adsorption energy. For comparison, E_{ads}(O) is −3.7 eV on the low index platinum

surface.[53] As shown previously by us, O_{ads}@MgO(001) is a non-magnetic system with O attached to the surface oxygen site.[12] The O–O bond is tilted towards the other nearest O atom of the MgO(001) surface, most likely due to the electrostatic interaction, as O_{ads} receives certain amount of charge from the substrate.[12,52] Upon the adsorption peroxo-like complex is formed. The electronic states of this complex are located below and above the MgO valence band.[12]

Similar to the CO adsorption, for O_{ads} we also find an enhanced chemisorption at the impurity site when compared to the O_{ads} formation on the defect-free MgO(001) terrace. The adsorption is extremely strong being strongest for B-doped MgO(001), for which E_{ads}(O) reaches −8.78 eV (Table 3). Considering ideal MgO(001) as the continuation of the given data set one can say that E_{ads}(O) increases linearly as the number of holes in the valence shell of the X^{2-} ions decreases (from B to O). The O_{ads}–dopant bonds are not vertical to the MgO(001) surface plane, and are found to be shifted towards the nearest Mg surface site (in the case of the O adsorption at the B impurity site) or the O surface site (all the other cases). As in the case of molecular CO adsorption, we see a significant charge transfer to O_{ads}, especially in the cases of B- and C-doped MgO(001) (Table 3), indicating once again that these impurities are exceptionally potent electron donors. Although we have shown that the exchange between O and X in the surface layer is significantly endothermic (Section 3.1) spontaneous exchange between X and O_{ads}, which would restore pristine MgO(001) has not been observed. Surface O NN sites to the dopants (Fig. 1) were found to be unstable for the O adsorption, as during the structural optimization O_{ads} migrated to the impurity sites in all the studied cases. However, a stable adsorption of O_{ads} was found at O NNN sites (Fig. 1) and the adsorption energies were found to be somewhat smaller compared to those on the pure MgO(001) surface.

Table 3. Energetic and structural parameters of the atomic O adsorption on pure and the X-doped MgO(001) surface. Total magnetizations (M) and the amount of the charge transferred to the adsorbate (ΔQ_O) are included. O NNN site is the oxygen center far from the impurity site.

Ads. site	System	E_{ads}(O) / eV	d(O–Su)[a] / Å	d(O–Su1)[b] / Å	M / μ_B	ΔQ_O / e
O site	O_{ads}@MgO(001)	−2.18	1.53	2.72	0	0.82
Impurity site	O_{ads}@B-MgO(001)	−8.78	1.25	2.09	0	1.98
	O_{ads}@C-MgO(001)	−7.39	1.31	2.70	2	1.94
	O_{ads}@N-MgO(001)	−5.08	1.40	2.63	1	0.93
O NNN site	O_{ads}@B-MgO(001)	-2.42	1.53	2.73	3	0.86
	O_{ads}@C-MgO(001)	-2.39	1.54	2.72	2	0.85
	O_{ads}@N-MgO(001)	-2.50	1.54	2.73	1	0.88

[a]Su denotes the surface atom at the CO adsorption site; [b]Su1 denotes the surface site towards which the O–Su bond is tilted (Mg site in the case of O adsorption on the impurity site of the B-MgO(001), O sites in all other cases)

The electronic structure of the O_{ads}@X-MgO(001) systems reflects the strong interaction of O_{ads} with the impurity sites (Fig. 7, left). The states of the impurity and the adsorbate overlap significantly. For the case of B-MgO(001) we see no states in the band gap and the system is not magnetic. For C- and N-doped MgO(001) the states in the band gap are present and the magnetization of the system has the same value as before oxygen adsorption. The magnetization of the system is mostly due to the p states of O_{ads} and dopant atom (Fig. 7, right). An interesting observation is that the p states of O_{ads} and the dopants also partially overlap with the MgO valence band, especially with its lower part.

344 It is also important to outline the difference in the interaction of CO and atomic O with the N-
345 doped MgO(001) surface. In the former case we see no bonding to the impurity site, while in the
346 latter one there is a significant enhancement of chemisorption properties as compared to pure
347 MgO(001). This suggests a possibility of making selective adsorbents and catalysts by a suitable
348 choice of the dopant.

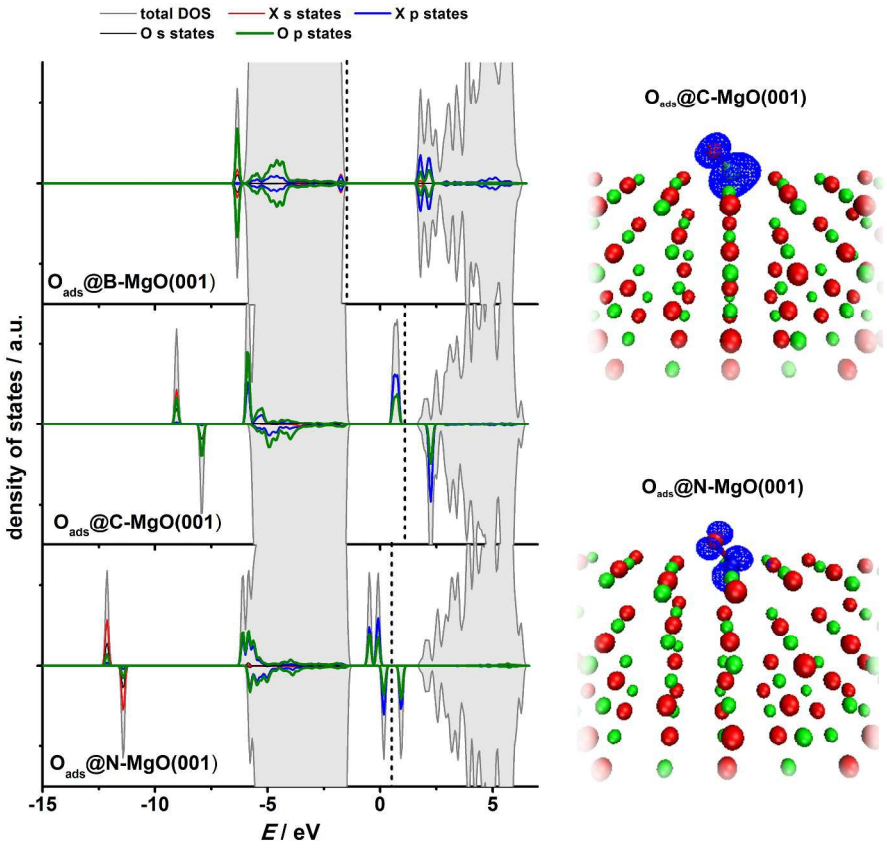

Figure 7. Left: Projected densities of states for the case of the atomic O adsorption at the impurity sites of the X-doped MgO(001) surface. Total densities of states are also included. Vertical lines indicate the highest occupied states. Right: 3D spin polarization maps, given as $\Delta\rho = \rho_{\uparrow} - \rho_{\downarrow}$, for the cases of the O adsorption on C- and N-doped MgO(001).

349

350 **4. Conclusions**

We have performed computational study of the B-, C- and N-doped MgO(001) surface, with the concentration of the dopants amounting to 1.56 at. % (12.5 at. % considering only the surface layer). We have found that the investigated dopants induce the appearance of the 2p like bands in the band gap of MgO that results in the system magnetization of 3, 2 and 1 μ_B for B-, C- and N-doping, respectively. The dopants are in the X^{2-} state and the ionic radii of these species are larger than the ionic radius of O^{2-}. As a consequence, all the three dopants prefer the surface sites instead of subsurface ones, as such a placement minimizes the strain of the host MgO lattice. The impurity sites are the centers of altered chemical reactivity. We probed the chemisorption properties of such doped surface with the CO molecule and atomic O. We have found that CO binds much stronger to B- and C-doped MgO(001) as the impurity sites serve as potent electron donors. The trend is similar for the case of atomic oxygen, for which we find E_{ads} to be −8.78 eV on B-doped MgO(001). The change of the local reactivity is seen in the first coordination sphere of the dopant. Our results suggest a possible way of producing a magnetic surface. They also suggest a way of tailoring the properties of the MgO(001) surface by a suitable choice of dopant to produce novel adsorbents and catalyst. This sets doped MgO as a versatile multifunctional material for numerous applications.

Acknowledgement

This work was supported by the Swedish Research Links initiative of the Swedish Research Council (348-2012-6196). The computational resources were provided by the Swedish National Infrastructure for Computing (SNIC).

References

1. H. L. Tuller and S. R. Bishop, *Annu. Rev. Mater. Sci.*, 2011, **41**, 369-398.

2. F. Calle-Vallejo, M. T. M. Koper and A. S. Bandarenka, *Chem. Soc. Rev.*, 2013, **42**, 5210-5230.

3. D. D. Vasić Anićijević, V. M. Nikolić, M. P. Marčeta-Kaninski and I. A. Pašti, *Int. J. Hydrogen Energy*, 2013, **38**, 16071-16079.

4. F. Yan, G. Xing, R. Wang and L. Li, *Sci. Rep.*, 2015, **5**, 9128, doi:10.1038/srep09128

5. D. A. Andersson, S. I. Simak, N. V. Skorodumova, I. A. Abrikosov and B. Johansson, *Proc. Natl. Acad. Sci.*, 2006, **103**, 3518–3521.

6. P. Poizot, S. Laruelle, S. Grugeon, L. Dupont and J-M. Tarascon, *Nature*, 2008, **407**, 496-499.

7. G. F. Fine, L. M. Cavanagh, A. Afonja and R. Binions, *Sensors*, 2012, **10**, 5469-5502.

8. M. Matsuoka, *Jpn. J. Appl. Phys.*, 1971, **10**, 736-746.

9. T. Lei, C. Ouyang, W. Tang, L.-F. Li and L.-S. Zhou, *Surf. Coating Tech.*, 2010, **204**, 3798–3803.

10. M. Amft and N. V. Skorodumova, *Phys. Rev. B*, 2010, **81**, 195443.

11. B. Yoon, H. Häkkinen, U. Landman, A. S. Wörz, J.-M. Antonietti, S. Abbet, K. Judai and U. Heiz, *Science*, 2005, **307**, 403-407.

12. I. A. Pašti, M. Baljozović and N. V. Skorodumova, *Surf. Sci.*, 2015, **632**, 39-49.

13. F. Frusteri, S. Freni, L. Spadaro, V. Chiodo, G. Bonura, S. Donato and S. Cavallaro, *Catal. Commun*., 2004, **5**, 611–615.

14. F. Frusteri, S. Freni, V. Chiodo, L. Spadaro, O. Di Blasi, G. Bonura and S. Cavallaro, *Appl. Catal. A: General*, 2004, **270**, 1–7.

15. I. A. Pašti, M. R. Baljozović, L. P. Granda-Marulanda and N. V. Skorodumova, *Phys. Chem. Chem. Phys.*, 2015, **17**, 9666-9679.

16. M. J. Stirniman, C. Huang, R. C. Smith, J. A. Joyce and B. D. Kay, *J. Chem. Phys.* 1996, **105**, 1295.

17. R. Nada, A.C. Hess and C. Pisani, *Surf. Sci.*, 1995, **336**, 353–361.

18. C.A. Scamehorn, N.M. Harrison and M.I. McCarthy, *J. Chem. Phys.*, 1994, **101**, 1547-1554.

19. S. Fernandez, A. Markovits and C. Minot, *J. Phys. Chem. C*, 2008, **112**, 16491–16496.

20. G. Pacchioni and N. Rösch, *J. Chem. Phys.*, 1996, **104**, 7329.

21. P. A. Žguns, M. Wessel and N. V. Skorodumova, *RSC Advances,* 2015, **5**, 94436 - 94445.

22. C. Zhang, B. Yoon and U. Landman, *J. Am. Chem. Soc.*, 2007, **129**, 2228–2229.

23. H.-J. Freund and G. Pacchioni, *Chem. Soc. Rev.*, 2008, 37, 2224-2242.

24. C. H. Yang, PhD thesis, 2010, Stanford University, CA.

25. L. Chun-Ming, G. Hai-Quan, X. Xia, Z. Yan, J. Yong, C. Meng, and Z. Xiao-Tao, *Chin. Phys. B* 2011, **20**, 047505.

26. M. Grob, M. Pratzer, M. Morgenstern and M. Ležaić, *Phys Rev B*, 2012, **86**, 075455.

27. M. Pesci, F. Gallino, C. Di Valentin and G. Pacchioni, *J. Phys. Chem. C*, 2010, **114**, 1350–1356.

28. I. R. Shein, A. N. Enyashin and A. L. Ivanovskii, *Phys. Rev. B*, 2007, **75**, 245404.

29. K. Kenmochi, M. Seike, K. Sato, A. Yanase and H. Katayama-Yoshida, *Jpn. J. Appl. Phys.*, 2004, **43**, 934-936.

30. K. Honkala, *Surf. Sci. Rep.*, 2014, **69**, 366–388.

31. J. P. Perdev, K. Burke and M. Ernzerhof, *Phys. Rev. Lett.*, 1996, **77**, 3865-3868.

32. P. Giannozzi, S. Baroni, N. Bonini, M. Calandra, R. Car, C. Cavazzoni, D. Ceresoli, G. L. Chiarotti, M. Cococcioni, I. Dabo, A. Dal Corso, S. Fabris, G. Fratesi, S. de Gironcoli, R. Gebauer, U. Gerstmann, C. Gougoussis, A. Kokalj, M. Lazzeri, L. Martin-Samos, N. Marzari, F.

Mauri, R. Mazzarello, S. Paolini, A. Pasquarello, L. Paulatto, C. Sbraccia, S. Scandolo, G. Sclauzero, A.P. Seitsonen, A. Smogunov, P. Umari, R. M. Wentzcovitch, *J. Phys.: Condens. Matter*, 2009, **21**, 395502.

33. R. Wyckoff, *Crystal Structures*, Interscience Publishers, New York, 1963.

34. H.J. Monkhorst and J.D. Pack, *Phys. Rev. B*, 1976, **13**, 5188-5192.

35. L. Bengtsson, *Phys. Rev. B*, 1999, 59, 12301-12304.

36. R. F. W. Bader, *Atoms in Molecules: A Quantum Theory*, Oxford University Press, 1990.

37. G. Henkelman, A. Arnaldsson and H. Jónsson, *Comput. Mater. Sci.*, 2006, **36**, 354-360.

38. W. Humphrey, A. Dalke, K. Schulten, *J. Mol. Graphics*, 1996, **14**, 33-38.

39. T. Gotoh, S. Murakami, K. Kinosita and Y. Murata, *J. Phys. Soc. Jpn.*, 1981, **50**, 2063-2068.

40. M. R. Welton-Cook and W. Berndt, *J. Phys. C*, 1982, **15**, 5691-5710.

41. D. L. Blanchard, D. L. Lessor, J. P. La Femina, D. R. Baer, W.K. Ford and T. Guo, *J. Vac. Sci. Technol. A*, 1991, **9**, 1814-1819.

42. N. V. Skorodumova, K. Hermansson and B. Johansson, *Phys. Rev. B*, 2005, **72**, 125414.

43. J. Carrasco, N. Lopez, F. Illas and H.-J. Freund, *J. Chem. Phys.*, 2006, **125**, 074711.

44. P.-O.Löwdin, *J. Chem. Phys.*, 1950, **18**, 365-375.

45. P.-O. Löwdin, *Adv. Quantum. Chem.*, 1970, **5**, 185-199.

46. V. E. Henrich, G. Dresselhaus and H. J. Zeiger, *Phys. Rev. B*, 1980, **22**, 4764-4775.

47. D.M. Roessler and W.C. Walker, *Phys. Rev.*, 1967, **159**, 733-738.

48. R. Valero, J. R. B. Gomes, D. G. Truhlar and F. Illas, *J. Chem. Phys.*, 2008, **129**, 124710.

49. P. Ugliengo and A. Damin, *Chem. Phys. Lett.*, 2002, **366**, 683-690.

50. R. Wichtendahl, M. Rodríguez-Rodrigo, U. Härtel, H. Kuhlenbeck and H.-J. Freund, *Surf. Sci.*, 1999, 423, 90-98.

443 51. B. Civalleri, L. Maschio, P. Ugliengo and C. M. Zicovich-Wilson, *Phys. Chem. Chem. Phys.*,

444 2010, **12**, 6382–6386

445 52. C. Di Valentin, R. Ferullo, R. Binda and G. Pacchioni, *Surf. Sci*., 2006, **600**, 1147-1154.

446 53. D. Vasić, Z. Ristanović, I. Pašti, S. Mentus, *Russ. J. Phys. Chem. A*, 2013, **87**, 2214–2218.